Turbulence in Rotating Convection

Kwing L. Chan
The Hong Kong University of Science and Technology,
Department of Mathematics
Clear Water Bay, Kowloon, Hong Kong, China
E-mail: maklchan@ust.hk

Abstract

Rotation plays vital roles in a great number of solar phenomena. Here we discuss results of a large eddy simulation study that illustrates the behavior of convective turbulence spanning over a wide range of Coriolis numbers.

Keywords: *Sun, rotation, convection, turbulence*

1. Introduction

Rotation has dominant effect on the convective turbulence in most of the solar convection zone. So far, a comprehensive understanding of the effect has not been achieved, and due to the complexity of the problem, realistic progress has to rely on numerical simulation. In an earlier paper (Chan, 2001), we have reported on an f-box study that covered the parameter space with a rather dense distribution of cases, so that trends can be clearly identified in the changing behavior of convection as the Coriolis number (Co = 1/ Rossby number) increases from 0 to some moderate value (≈ 7). For a review of the literature, the readers are referred to the paper by Brummell et al. (1996).

In the last couple of years, we have made higher resolution calculations ($70 \times 70 \times 80$ *vs* $35 \times 35 \times 39$ meshes) that allow us to extend the range of Co to higher values (since the sizes of large eddies decrease with increasing Co; see later discussion). Here the discussion is focused on the changing behavior of the turbulence across the different values of Co (≈ 0 to 15.6); the latitude is fixed at 22.5°.

2. The Model

A 'f-box' is a three-dimensional, rectangular, horizontally periodic, region that approximates a small piece of the global rotating convection zone. In this region, the angle between the rotation vector and the vertical direction is considered to be constant (the colatitude). In our Cartesian system, the x-, y-, z- axes are

north-to-south, west-to-east, and radially outward, respectively (a right-handed system). The gas is ideal and the total stratification is about 5 pressure scale heights. The units are chosen so that the total depth, the pressure, density, and pressure at the top are all equal to 1 (in these units, sound speed $= \sqrt{\gamma} \approx 1.29$). The top of the convection zone is at the height 0.95, above which lies a marginally stable layer to soften the impact of the turbulence with the upper boundary. Further details of the model can be found in Chan's paper.

In this short article, we consider eight cases which have rotation rates Ω sequentially chosen at 0, 1/8, 1/4, 1/2, 1, 3/2, 2, and 3. Correspondingly, the Coriolis number, defined to be $\Omega \int dz / \int v'' dz$ where v'' is the rms velocity (with contribution of the mean already subtracted), takes on the approximate values 0, 0.7, 1.3, 2.6, 5.4, 8.3, 11.1, and 15.6. The resolution may not be sufficient for the fastest rotating case, but we include it here for comparison.

3. Dependence of the Turbulence on Rotation Rate

3.1. Flow patterns

Figure 1 shows horizontal cuts of instances of the vertical velocity field v_z at a number of depths for the different cases. The dark lanes show downflow regions. Roll structures are prominent, and there is a transition in the roll alignment from north-south to west-east between $\Omega = 1/8$ and 1/4. The east-west alignment can be explained by the linear analysis of Hathaway et al. (1979), and the transition to the north-south alignment can be understood as the growing dominance of the Taylor-Proudman effect at higher Co. The separation of the downflow lanes decreases with increasing Co.

Figure 2 shows the vertical component of the vorticity $\zeta'_z = (\vec{\nabla} \times \vec{v}')_z$. Note that $()'$ denotes that the fluctuating quantity already has the mean subtracted. Both positive and negative vorticities concentrate along the downflow lanes, but the positive kind is more prominent. Figure 3 shows the vertical contribution to the helicity, $v_z \zeta'_z$. This part of the helicity also shows a tendency to concentrate in the downflow lanes, but its distribution is more spotty than the vertical vorticity. The spots are primarily negative and prominent only near the top of the convection zone.

Figure 4 illustrates that the rolls are tilted from the horizontal direction. The roll axes are more or less in alignment with the rotation vector. Before the stream lines are generated, the horizontal mean flows have been subtracted from the velocity field.

3.2. Statistics of the velocity field

Figures 5 and 6 show the horizontal and temporal mean of the meridional (north-south) and zonal (west-east) velocities, respectively. For small Co, the mean velocities have shear-like distributions. As Co gets larger, the shear region shrinks towards the top. The senses of the shears below the top of the convection zone are negative (velocities dropping outward). The depth extent of the shear region is related to the local Coriolis number ($\equiv \Omega H_p/v''$ where H_p is the local pressure scale height) whose distributions are plotted in Figure 7. The shears are confined to regions with the local Coriolis number below 1. The vertical averaging of the local Coriolis number defined here yields the values 0, 0.19, 0.35, 0.73, 1.6, 2.5, 3.4, 4.6 for the eight sequential cases. They are different from the Co defined earlier; there is arbitrariness in the choice of the characteristic velocity and length scales.

The symmetric Reynolds stress tensor contains six independent components. The diagonal ones are the mean square velocities, and the off-diagonal ones are covariances of different velocity components. Dynamically the diagonal stress components act as turbulence pressure along different directions, and the off-diagonal ones produce momentum transport. One interesting result in the f-box configuration is that the mean zonal flow is driven only by the vertical-meridional component of the Reynolds stress; components that carry the zonal momentum do not participate in the averaged momentum balance. Figure 8 shows the distributions of the rms vertical velocity. Higher rotation rates tend to suppress this component of velocity. Figure 9 shows the rms meridional velocity, the rms zonal velocity behaves similarly (except in the fastest rotating case whose results may not be reliable).

Figure 10 shows the correlation coefficient of the two horizontal velocities (remember that the means have been subtracted). Between the Co values 0.7 and 2.6, there is a change of sign in the correlation, almost at all depths. At the Co value 1.3, the situation is transitional. Figure 11 shows the correlation coefficient of the vertical and meridional velocity fluctuations. Note the general presence of positive peaks near the top of the convection zone in all of distributions; they are responsible for producing the negative dips in the zonal velocity near the top, through the meridional momentum equation. Figure 12 shows the correlation of the vertical and zonal velocity fluctuations. Though negative (as expected) when the Co is small, the correlation drops in magnitude when Co gets large, and eventually regions of positive correlation show up.

4. Summary

Results of the higher resolution calculations presented here are generally in agreement with those obtained by the low resolution calculations presented in the earlier paper. The higher resolution allows us to view the flow fields more clearly. That also makes possible the pushing of Co to higher values, further consequences of which are to be explored in a later paper.

Acknowledgments

I would like to thank the SOC/LOC of this NATO Workshop for the support of local expenses. The research is supported by the RGC of Hong Kong.

References

Brummell, N. H., Hurlburt, N. E., & Toomre, J. 1996, *Astrophys. J.* , 473, 494

Chan, K. L. 2001, *Astrophys. J.* , 548, 1102

Hatherway, D. H., Gilman, P. A., & Toomre, J. 1979, Geophys. Astrophys. Fluid Dyn., 13, 289

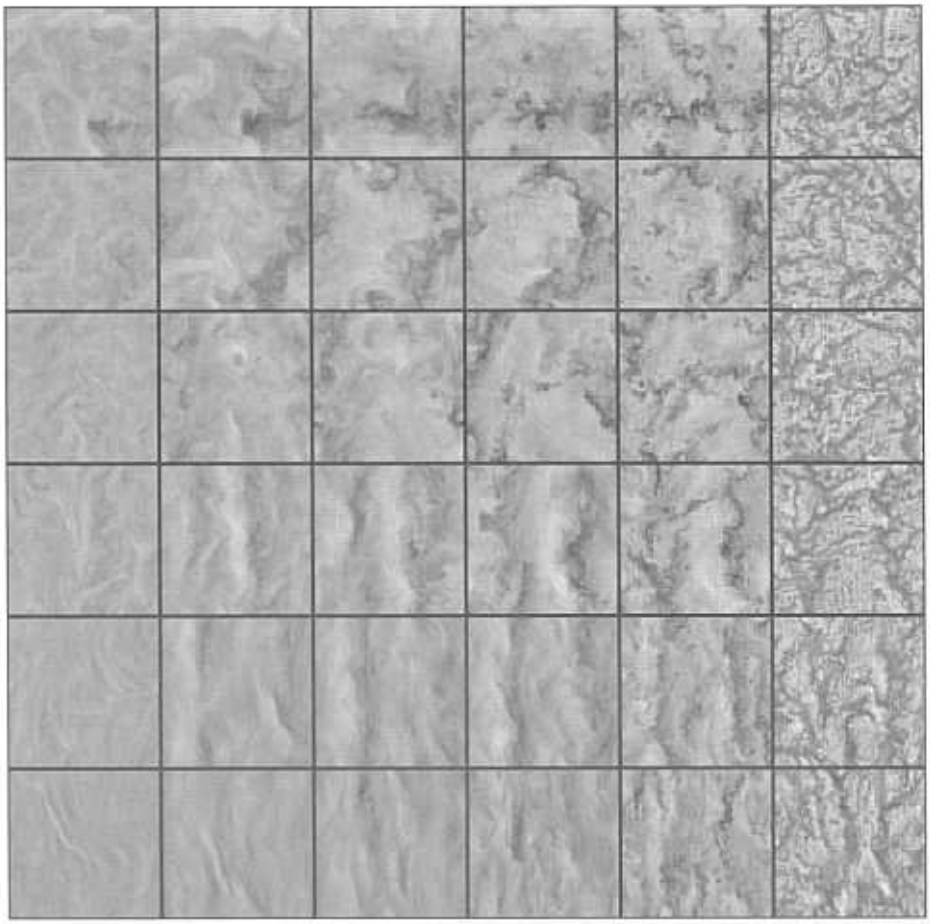

Figure 1: From top to bottom, the rows show instances of the vertical velocity field for the cases with $\Omega = 1/8,\ 1/4,\ 1/2,\ 1,\ 2,\ 3$, respectively. Each column shows horizontal cuts of the fields at a fixed depth. From left to right, the depths go from deeper to shallower. The vertical and horizontal directions represent the north-south and east-west orientations, respectively.

Figure 2: Horizontal cuts of the vertical vorticity field (i.e. $(\vec{\nabla} \times \vec{v}')_z$) for the same instances and cases as those in Figure 1.

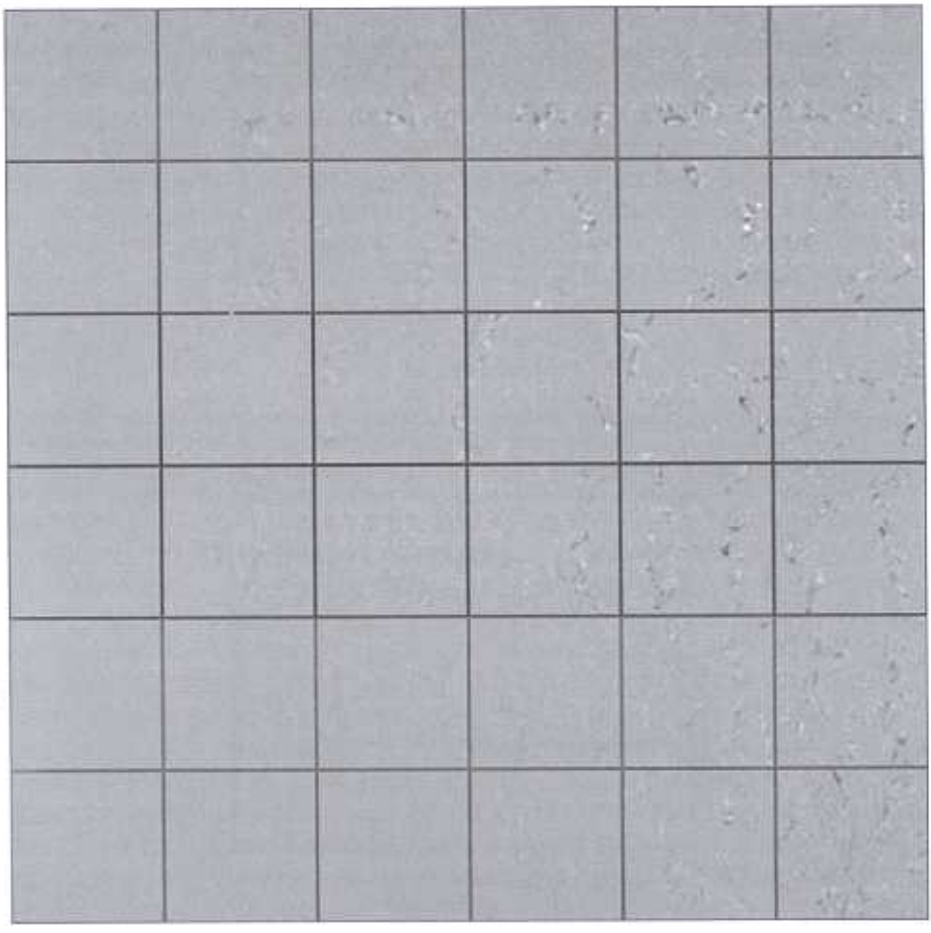

Figure 3: Horizontal cuts of the vertical contribution to the helicity field (i.e. $v_z(\vec{\nabla} \times \vec{v})_z$) for the same instances and cases as those in Figure 1.

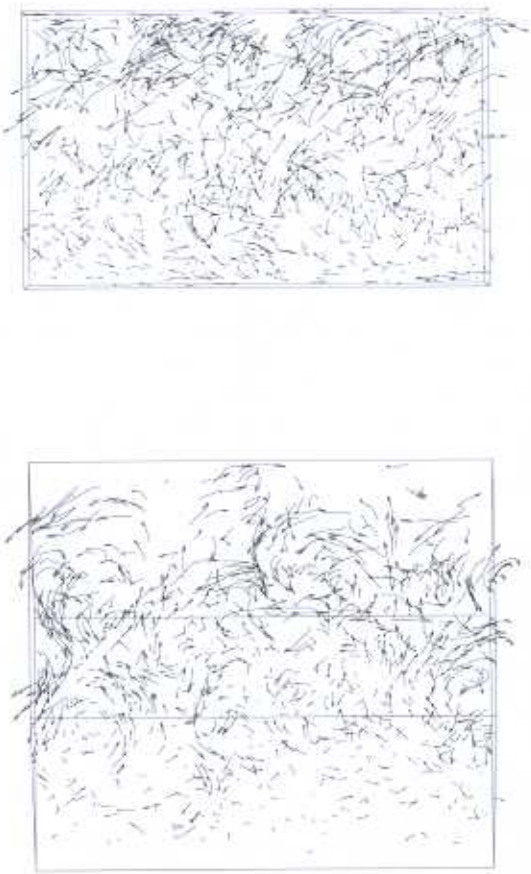

Figure 4: Streamlines of the turbulence velocity field (mean flows eliminated) in an instance of the $\Omega = 2$ case. *Upper panel*: A view taken from the west side of the box towards east. *Lower panel*: A view taken from the south side and 22° below the horizon, towards the north and at an angle 68° from the vertical direction; the projected streamlines indicate circular roll motions.

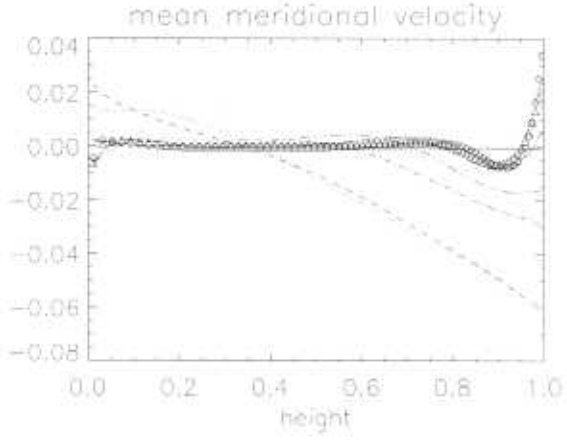

Figure 5: Vertical distributions (profiles) of the horizontally and temporally averaged mean meridional flow. The $\Omega = 0$, 1/8, 1/4, 1/2, 1, 3/2, 2, 3 cases are represented by the solid, dotted, short dashed, dot-dashed, triple-dot-dashed, long dashed lines, the triangles, and rhombus, respectively. All later figures use the same symbols to identify the cases.

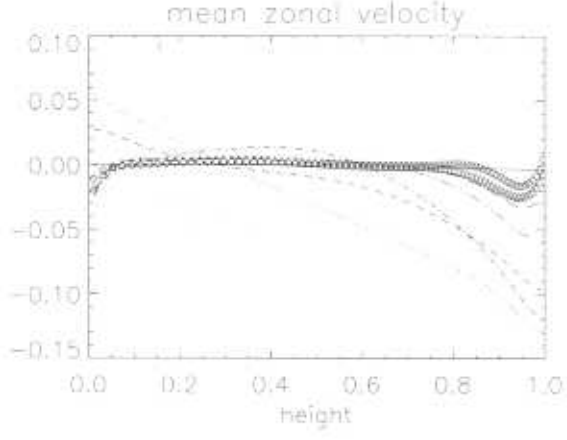

Figure 6: Profiles of the horizontally and temporally averaged mean zonal flow. All show dips near the top of the convection zone.

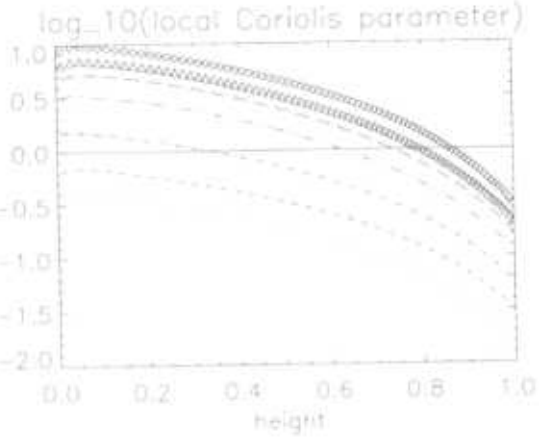

Figure 7: log_{10} of the local Coriolis number, defined as $\Omega H_p/\nu''$. The characteristic length scale is chosen to be the local pressure height H_p.

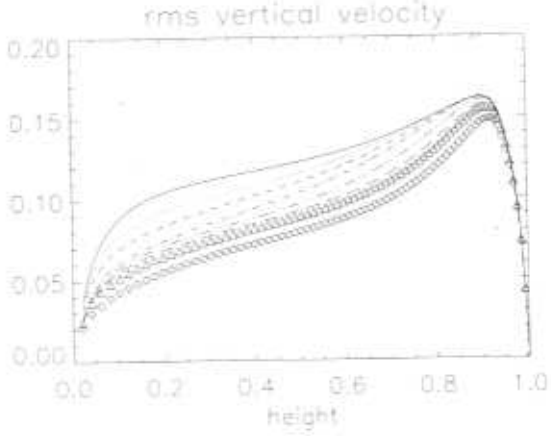

Figure 8: Profiles of the rms vertical velocity. Rotation tends to suppress this velocity.

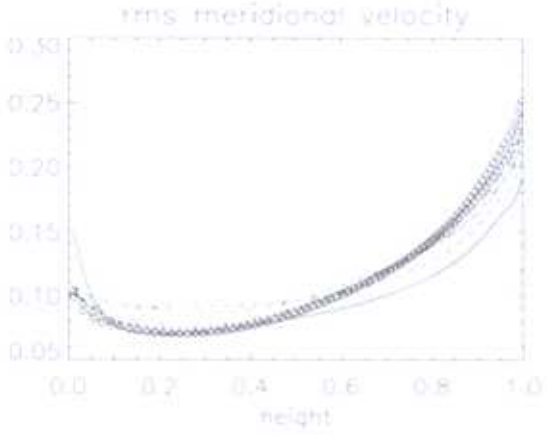

Figure 9: Profiles of the rms meridional velocity.

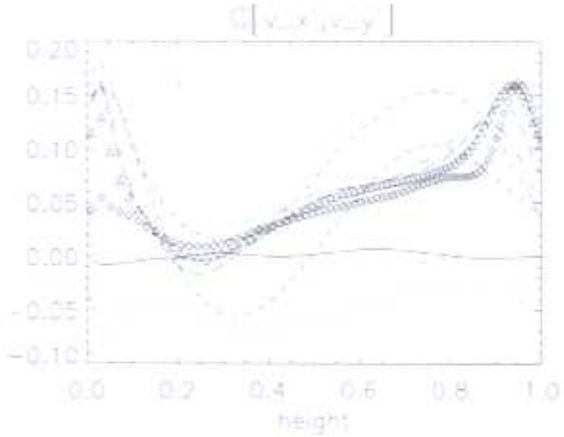

Figure 10: Profiles of the correlation coefficient of the two horizontal velocity fluctuations. There is a change of sign between the distributions for the low and the high Co values.

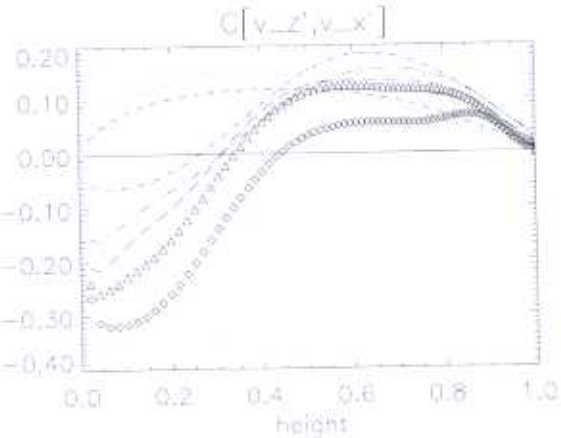

Figure 11: Profiles of the correlation coefficient of the vertical and meridional velocity fluctuations. Note the general presence of a positive peak in the upper region of the convection zone.

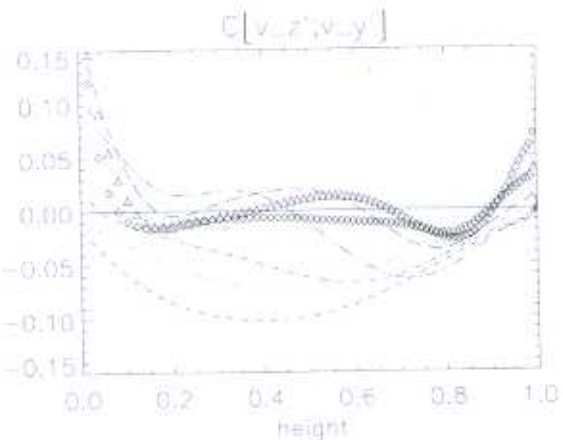

Figure 12: Profiles of the correlation coefficient of the vertical and zonal velocity fluctuations. Its value is not always negative.